




Article

A Secure Traffic Police Remote Sensing Approach via a Deep Learning-Based Low-Altitude Vehicle Speed Detector through UAVs in Smart Cities: Algorithm, Implementation and Evaluation

Ata Jahangir Moshayedi ¹, Atanu Shuvam Roy ², Alireza Taravet ³, Liefia Liao ¹, Jianqing Wu ^{1,*}
and Mehdi Gheisari ⁴

¹ School of Information Engineering, Jiangxi University of Science and Technology, No. 86, Hongqi Ave., Ganzhou 341000, China

² Department of Computer Science and Engineering, Indian Institute of Technology, Kanpur 208016, India

³ Deimos Space, Oxford OX11 0QR, UK

⁴ Department of Cognitive Computing, Institute of Computer Science and Engineering, Saveetha School of Engineering, Saveetha Institute of Medical and Technical Sciences, Chennai 602105, India

* Correspondence: jianqing.wu@jxust.edu.cn

Abstract: Nowadays, the unmanned aerial vehicle (UAV) has a wide application in transportation. For instance, by leveraging it, we are able to perform accurate and real-time vehicle speed detection in an IoT-based smart city. Although numerous vehicle speed estimation methods exist, most of them lack real-time detection in different situations and scenarios. To fill the gap, this paper introduces a novel low-altitude vehicle speed detector system using UAVs for remote sensing applications of smart cities, forging to increase traffic safety and security. To this aim, (1) we have found the best possible Raspberry PI's field of view (FOV) camera in indoor and outdoor scenarios by changing its height and degree. Then, (2) Mobile Net-SSD deep learning model parameters have been embedded in the PI4B processor of a physical car at different speeds. Finally, we implemented it in a real environment at the JXUST university intersection by changing the height (0.7 to 3 m) and the camera angle on the UAV. Specifically, this paper proposed an intelligent speed control system without the presence of real police that has been implemented on the edge node with the configuration of a PI4B and an Intel Neural Computing 2, along with the PI camera, which is armed with a Mobile Net-SSD deep learning model for the smart detection of vehicles and their speeds. The main purpose of this article is to propose the use of drones as a tool to detect the speeds of vehicles, especially in areas where it is not easy to access or install a fixed camera, in the context of future smart city traffic management and control. The experimental results have proven the superior performance of the proposed low-altitude UAV system rather than current studies for detecting and estimating the vehicles' speeds in highly dynamic situations and different speeds. As the results showed, our solution is highly effective on crowded roads, such as junctions near schools, hospitals, and with unsteady vehicles from the speed level point of view.

Keywords: vehicle detection; vehicle speed estimation; transportation; unmanned aerial vehicle; deep learning; remote sensing



Citation: Moshayedi, A.J.; Roy, A.S.; Taravet, A.; Liao, L.; Wu, J.; Gheisari, M. A Secure Traffic Police Remote Sensing Approach via a Deep Learning-Based Low-Altitude Vehicle Speed Detector through UAVs in Smart Cities: Algorithm, Implementation and Evaluation. *Future Transp.* **2023**, *3*, 189–209. <https://doi.org/10.3390/futuretransp3010012>

Academic Editors: Ouri E. Wolfson and Shunde Yin

Received: 1 October 2022

Revised: 14 January 2023

Accepted: 28 January 2023

Published: 3 February 2023



Copyright: © 2023 by the authors. Licensee MDPI, Basel, Switzerland. This article is an open access article distributed under the terms and conditions of the Creative Commons Attribution (CC BY) license (<https://creativecommons.org/licenses/by/4.0/>).

1. Introduction

Unmanned aerial vehicles (UAVs) are increasingly used for remote sensing (RS) applications and are a relatively new category of robots in broader (commercial) use [1]. The small size, flexible movement, and good control of UAVs [2] combined with the vision systems [3] open a new gate for measuring and capturing data remotely. Recently, RS applications using UAVs have been used for various tasks, such as thermography timing of different thermal orthomosaics and photographs [4], boundary detection between land

parcels [5], complex and irregular field shape [6], accuracy measurement [7] or validating for utilizing multi-temporal color images [8], and precision agriculture to optimize crops and facilities crops management [9]. However, visual/object tracking to locate, detect, and define objects [10] via UAV images is still challenging, even with state-of-the-art deep learning models (RESNET, Mobilenet, Efficient Net etc.) in the field of computer vision. Today, deep learning algorithms reach performance close to human experts in many applications, e.g., traffic surveillance, accident avoidance, traffic intersections [3,10], autonomous vehicles, and intelligent transport systems. In the related literature, Retina Net, FCOS, and YOLOv3 (YOLO-v3, YOLO-v3-spp and YOLO-v3-tiny) [11,12], Faster R-CNN [12–14], multi-perspective convolutional neural network R-CNN [15], and hierarchical Bayesian algorithm [16] are proposed for vehicle detection based on satellite data or stationary vision systems. Based on the authors' knowledge, there are few studies so far about the combination of UAV, visual/object tracking and speed detection. Moranduzzo et al. [3] proposed a method based on scale-invariant features transform (SIFT) for vehicle speed estimation in UAV imagery. The process begins with registering two successive images belonging to a sequence acquired by the UAV at a height of 200 m. Their results show that the proposed method generates 80.0% accuracy for car detection on the images acquired at a height of 200 m. Afifah et al. [17] estimated vehicle speed using Euclidian distance. As the first step in their processing chain, all the images are transformed with warp perspective to align them with a global coordinate. Then, they are converted to grayscale images and blurred with a gaussian function. Finally, after performing background subtraction and comparing and thresholding the images, the vehicle speed is estimated by comparing each vehicle with itself in the next frame using Euclidian distance. The accuracy of their proposed approach is 92%. However, although very low altitude (<10 m) UAV-based car speed detection systems can be very effective, a detailed analysis of them has not been performed yet. The present paper aims to demonstrate the potential of deep learning approaches in newly proposed car speed detection systems using low-altitude UAV data to help traffic safety and security in smart cities. This paper makes the following contributions:

1. A more reliable and secure solution to verify vehicle speed using drones instead of current studies is offered.
2. Providing an effective alternative method against the many reported cases of accident damages and injuries for police officers as well as fixed traffic cameras.
3. Introducing the quick speed check system, which can be used in places with limited access and in conjunction with the available speed detection system.
4. A low-altitude drone equipped with a Mobile Net-SSD method to measure vehicle speed and a network connection capability was employed to implement our approach.
5. To achieve our solution, a low-altitude drone equipped with the Mobile Net-SSD algorithm was used to detect the speed of vehicles and has the ability to connect to the traffic police.
6. Several scenarios were taken into account in various conditions, such as road intersections and settings with abrupt speed changes, to provide more accurate findings.
7. To increase the solution's speed detection accuracy, the effective cases were tested and calibrated using a drone. The system was run on Raspberry PI4B for its faster-processing speed, and memory capabilities, such as capacity and bandwidth, benefit the deep learning-based computer vision module to run smoothly.
8. In addition to our earlier contribution, which was already discussed above, a movable camera system was mounted on top of the drone, offering a number of opportunities to assess our solution at various altitudes along the X and Y axes.
9. In addition, a graphical user interface (GUI) was designed and implemented that allows us to record the environment's status, identify problematic conditions based on speed parameters, and send alarms to the appropriate authorities was built and put into place. Additionally, we may manage the camera's status, including its movement, through the GUI.

In general, the authors of this article believe that based on the variety of tests conducted in real cases and measurements performed. The results mentioned in the following sections and the satisfactory performance of the introduced method and system can effectively solve various scientific problems. The rest of the sections are organized as follows. Section 2 introduces the system setup and methodology used for vehicle detection, tracking, and speed estimation. Section 3 provides experimental results, followed by a discussion in Section 4. Conclusions and potential paths for future work are given in Section 5.

2. Materials and Methods

According to the review of the past articles [18] and the investigation of the remaining cases, vehicle speed detection systems include challenges and difficulties that need to be reviewed and updated. Some of the most important limitations can be considered as follows: Structural limitations, e.g., installing cameras at a height of 3–5 m vertically on the road surface, lead to insufficient visibility on winding roads [17], the cost and maintenance limitations of fixed cameras, which cause their limited use in places with the short-term investigation times, special uses, such as schools and hospitals, which have a lower speed limit than other places, and the possibility of using various processors [19] based on the Internet of Things(IOT), considering the good accuracy and speed for vehicle speed detection and tracking mission [18]. Therefore, according to the mentioned cases, future urban and traffic management requires the use of capabilities, such as maneuvering and fast movement, of UAVs, regardless of the type and characteristics of the cameras used. The methodology of the paper is divided into four sections: system setup, which is about the proposed hardware for the speed sensing system; vehicle detection and tracking, which is the full description of the method and algorithm used for vehicle detection and tracking section of the system. The vehicle speed estimation section fully describes the VASCAR approach used for vehicle speed estimation. The system calibration section demonstrates the sets of indoor and outdoor system calibration. The whole assembly is meant to capture, read, and analyze the raw video input from the Raspberry Pi camera and give output in real-time (Figure 1).

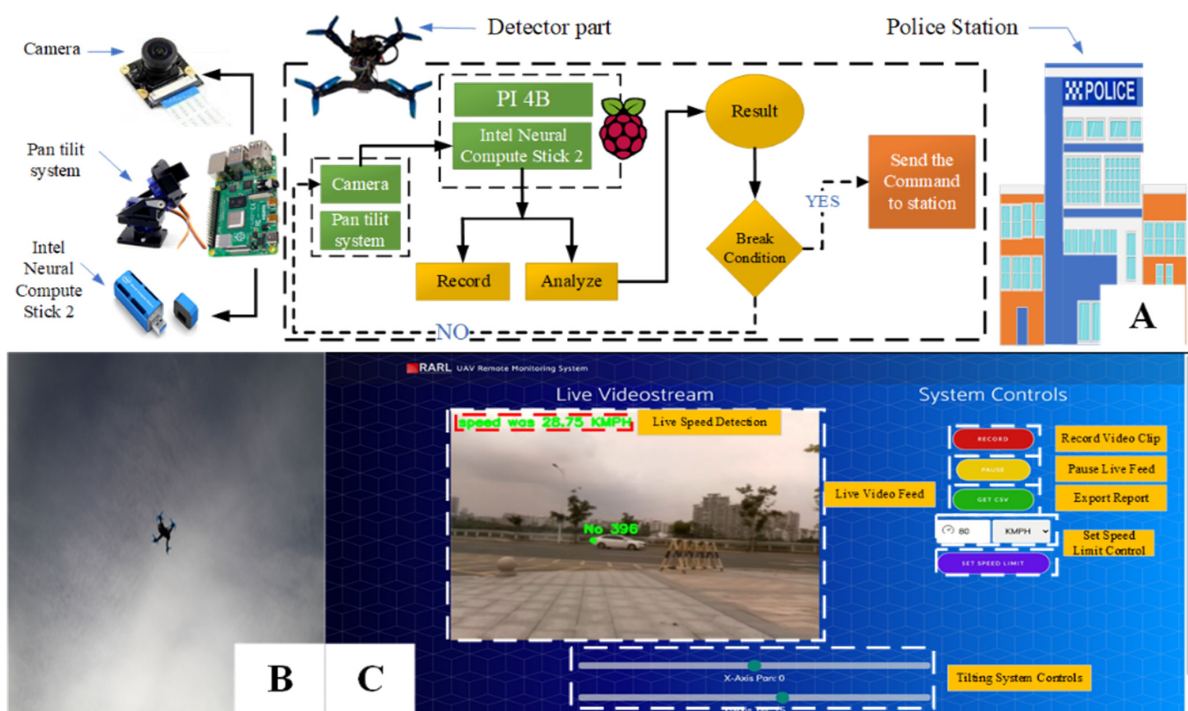


Figure 1. Proposed speed detection system (A) the total system scheme and logic, (B) the proposed UAV, (C) the system performance and designed GUI.

2.1. System Materials

The proposed speed sensing system consists of a UAV, CPU, and vision system, as well as an object and speed detector along with a web-based GUI (Figure 1A). The UAV (Tarot TL280H/Air 2205 2000 KV/10 × 4.5 mm) includes a control board (ArduPilot APM 2.8-3DR Robotics, USA), Motors and speed control driver (T-Motor Air 15A_China), GPS (Ublox NEO-7M u-blox, Swiss), radio controls (TX: NET-Q118G, China), radio transmitter (RG831B, 8ch 2.4 GHz, China), and battery (PULSE 2250 mAh 3S LiPo Battery, China). The vision system consists of a Raspberry Pi camera with 1.3–5 MP maximum photograph resolution (2592 × 1944), a Pan-Tilt system containing two servo motors, which can move between +90° and −90° (vertically and horizontally) to move the camera and have a controllable view, and an Intel neural compute stick 2. The Intel neural compute stick 2 is the next generation of Intel's USB plug-and-play development kit for AI and deep learning technology, powered by Intel's Movidius Myriad X Visual Processing Unit (VPU) [20]. It can be used for real-time analysis of raw video footage from cameras, which normally takes lots of time on a traditional CPU. Another reason for using this is its unique workload-specific hardware acceleration that minimizes data movement. The vision section is attached to a Raspberry Pi 4 minicomputer via a USB port. The Raspberry Pi processor and its camera (Pi camera) have been used in various Internet of Things projects and are recognized as a trustable platform [21]. Among the variety of Raspberry Pi types, the Pi 4 type has been chosen as it is the latest available version and supports high speed in data processing, which is a mandatory requirement for this research. It should be mentioned as the quad needs light accessories to continue the flight of the Pi camera, along with their small weight, size and processing capability, the Broadcom CPU was selected, which makes this camera unique [22]. The tilting system is connected to the Raspberry Pi GPIO connectors mounted on the UAV (Figure 1B). As Figure 1 shows, the whole system works such that after running the program inside the PI, the camera, as the first part of the sensing system, captures the video stream and feeds it into the raspberry pi computer. The program records and analyzes the video. Then, the user inside the designed web-based GUI (Figure 1C) can monitor the live detection process, and by defining the speed value inside the GUI, any car that passes the limit receives the alarm. The design GUI (Figure 1C) has the other feature to record, pause, and export the detected car report, along with a tilting system to control the camera attached to the UAV.

2.2. Deep Learning Model Architecture

Inside the design, the Single Shot Multibox Detector Mobile Net (SSD-Mobile net) was used as the deep learning model. This model is designed based on (Depth wise Separable Convolutions), which are separated into different CONV layers, one for filtering and one for integrating. In other words, SSD object detection comprises two sections, extracting feature maps, and applying convolution filters to detect objects.

In this research Mobile Net-83 SSD model was selected due to features. such as good accuracy for target detection [23], small size and high speed with real-time processing performance [24], the ability to detect the object in one shot with the Multibox detector [25], along with the ability to implement on embedded system platforms. In addition, this model can detect the object [26] that is supposed to tilt the camera UAV in two axes, according to the experimental target [27]. The suggested SSD Mobile Net model is shown in Figure 2.

As Figure 2 shows, the Mobile Net model aims to assign a default filter to each neural input channel for setting up the extraction of features. A (1 × 1) pointwise convolution follows next to integrate the outcome of the depthwise convolution. The batch norm comes into each of these separable layers. ReLU nonlinearity anticipates that the final (FC) layer that feeds into a SoftMax layer will be classified as having no nonlinearity. Unlike classic CNN, Mobile net's filters analyze each color channel separately before combining the three outputs into a single value. This factoring has a significant impact. In the developed method, features from the input photos are extracted using (32 and 64) filters with sizes of

(5×5) before two max-pooling (pool size = 2). More details about the model can be found in [28].

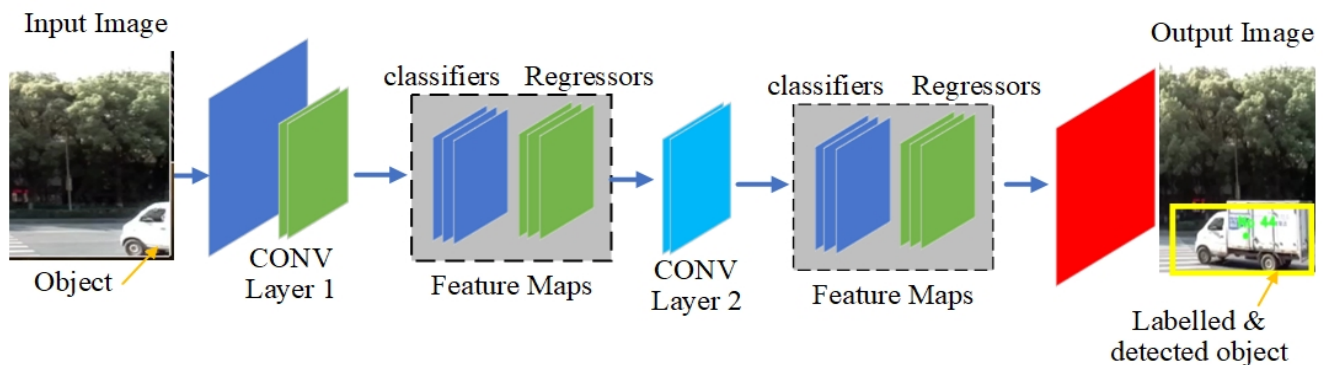


Figure 2. The single shot multi-box detector mobile net (SSD-mobile net) model structure.

2.3. Vehicle Detection and Tracking

The proposed system follows the described process in Figure 3. As shown, the main steps of work consist of initialization, which includes initializing the camera for live stream, DNN (SSD-mobile net) calling to perform in the vehicle's detection section, and speed calculation.

Figure 3 depicts the proposed vehicle speed estimation process which starts by receiving the video stream from the camera to calculate the speed of each tracked vehicle.

The program takes in each frame of the livestream footage and runs it through a pre-trained deep-learning model. As shown, after initialization and getting the object frame called, the OpenCV DNN converts the image blob and performs detection by confidence evaluation. The confidence evaluation means the strictness of matching each vehicle. The lower the minimum confidence specified, the less will be the detection accuracy. If the confidence of the detected vehicle is more than the minimum confidence (70%), then the vehicle will be indexed into memory and classified into a vehicle category followed by the setting of a bounding box and its position set to be tracked in the subsequent frames on the live feed. If the confidence of the tracked vehicles is less, the object's last position will be updated. Then, the new vehicle will be tracked, and the loop will keep going. The model contains classification methods for all types of vehicles, such as cars, buses, trucks, etc. Meanwhile, vehicle tracing occurs as the vehicle moves across consecutive frames and calculates and declares the speed using the formulas explained in this section.

2.3.1. Vehicle Detection Approach

The vehicle detection phase consists of a multi-step process that relies on the existing object centroid calculated in the proposed system to confirm and define the new object (Figure 4).

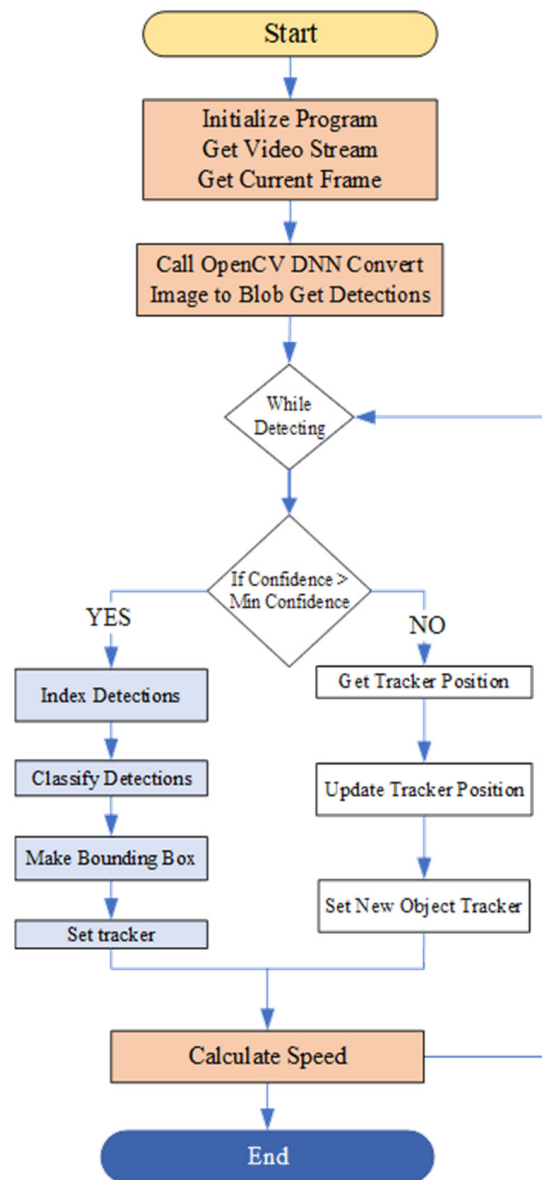


Figure 3. The proposed vehicle speed estimation process.

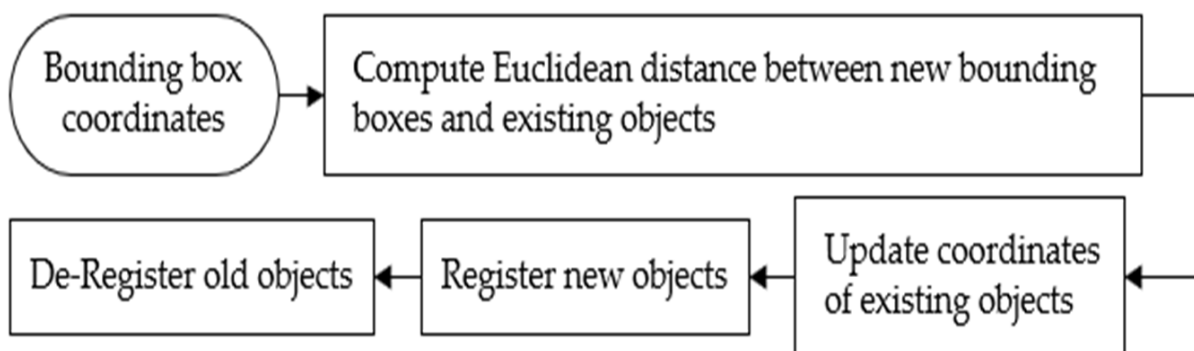


Figure 4. The schematic view of the vehicle detection and tracking algorithm.

The first task in the vehicle detection and tracking phase is to identify the objects and build bounding boxes around them. For this purpose, all three bands (Red, Green, and Blue) of each frame of the video are normalized using the following equations (Equation (1)):

$$\text{NormBand} = \frac{(\text{Band} - \mu_{\text{BAND}})}{\sigma} \quad (1)$$

where Band is band values, and μ_{BAND} is the mean of each red, green, and blue Band, respectively, σ is the scaling factor for normalization. After normalization, Mobile Net-SSD is used for detecting vehicles. Mobile Net-SSD is a Single-Shot multi-box Detection (SSD) network intended to perform object detection. The vehicle detection and tracking system loops over all detected vehicles, add a bounding box around them and then calculates the centroid of the boxes. After the bounding box coordinates are extracted, the Euclidean distances between the new and old bounding boxes are calculated. Each video frame can have a different position of the previously tracked object, leading to different boxes assigned to the same object in different frames. To avoid this, the distance between the new object in the next frame and the old object in the last frame is calculated using the following equation (Equation (2)):

$$d(x, y) = \sqrt{\sum_{i=1}^n (y_i - x_i)^2} \quad (2)$$

where x and y are x and y coordinates, respectively, and i is the instance. For instance, suppose that the last object detected in the frame is F_t , and the newly detected object is F_{t+1} (where it is the current frame). If the old and newly detected objects refer to the same object, then the distance between F_t and F_{t+1} will be less than a new object's length. Hence, the algorithm associates newly detected objects with previous ones' consecutive frames and updates their position. In the last step, tracked vehicles that have not been visible in 4 frames are removed and not tracked anymore.

2.3.2. Vehicle Speed Estimation Using an Improved VASCAR approach

This study's vehicle speed estimation model is based on an improved Visual Average Speed Computer and Recorder (VASCAR) method [29]. This method is based on timing and the known distance between two fixed points on the road, as shown in Equation (3). When a car passes the first reference point, the detector triggers the timer and captures the time until the car passes the last point to calculate velocity.

$$\text{Vehicle speed} = \frac{\text{distance between Points (A - B)}}{\text{time}} \quad (3)$$

In the case of human operation, this method is severely limited by human error and delayed reaction. This research considers four instead of only two points and automatically calculates the velocity between the reference points. The standard VASCAR is calculated based on three points, while in the improved VASCAR, four measurements have been considered to calculate velocity. The measurement process is shown in Figure 5.

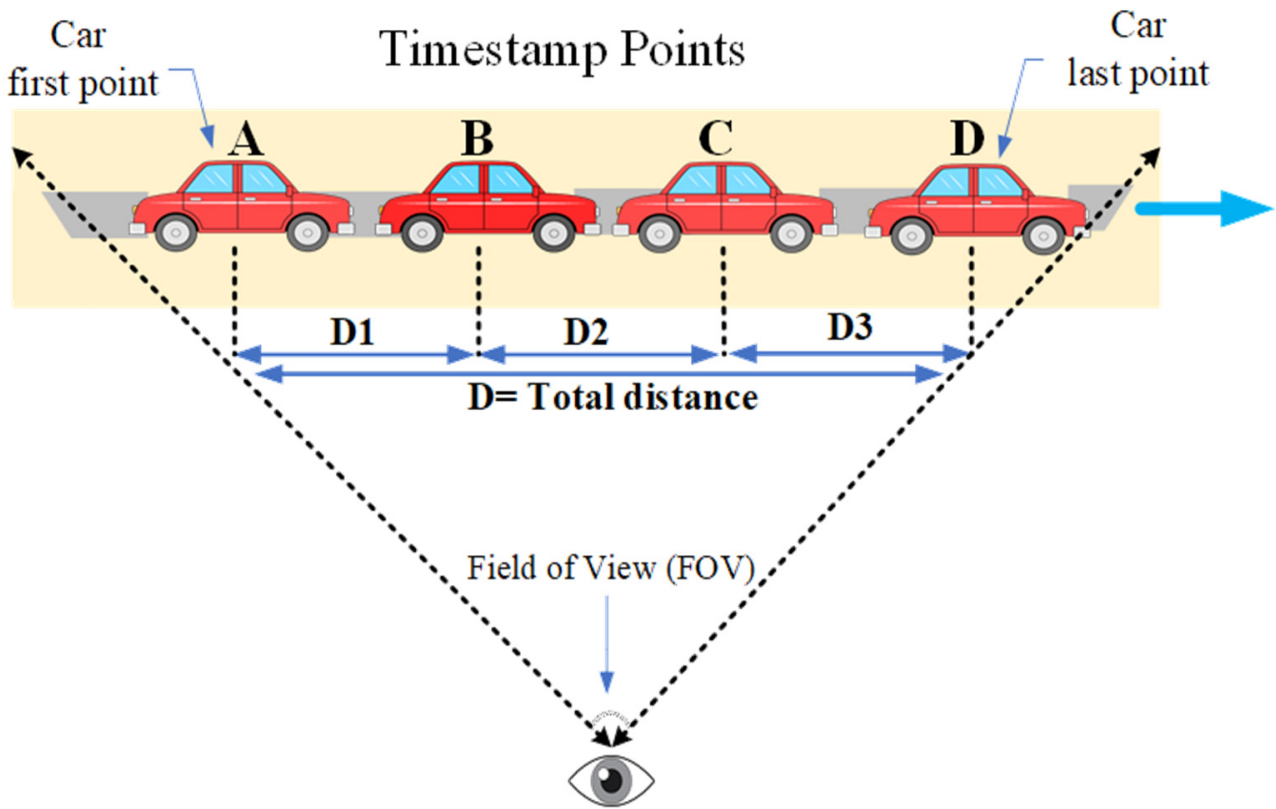


Figure 5. Schematic view of the VASCAR approach in different location of A to D.

As shown in Figure 5, the car was detected at the specified point with a known distance. The system calculates the field of view based on the distance from the road it observes. The speed estimation system divides the whole frame into four points, considering the frame points in the video to track the object. When a car passes reference point A, the detector triggers the timer and captures the time until the car passes point D. This automatic approach overcomes human error and delayed reaction that might occur in the case of human operation. The calculations are shown in Equation (4).

$$\text{Average Speed (km/h)} = \left(\frac{D_1}{t_1} + \frac{D_2}{t_2} + \frac{D_3}{t_3} / 3 \right) \times 3.6 \tag{4}$$

where D_1 is the distance between points A–B in meters at t_1 second, the distance D_2 between points B–C as t_2 second, and the points C–D distance as D_3 meter with t_3 second. As Figure 5 shows, tracking an object in four points results in three distances included in the relationship to calculate the average. In the next step, the system calculates the field of view (FOV) based on the distance from the object. From the system point of view, at the same time, new vehicles are constantly being tracked and registered, and old objects are being deregistered. Meanwhile, the improved VASCAR algorithm is applied to each tracked vehicle. In the second phase, the system initializes the estimated speed list, loops over all the pairs of points, and estimates the speed of each object. Then, it calculates the number of pixels between centroids in points and converts it to real-world distance(meters) as the pixel per meter (PPM) in Equation (5) and calculates the vehicle’s average speed.

$$\text{PPM} = \frac{\text{Distance Constant}}{\text{Frame Width}} \tag{5}$$

Equation (6) calculates the pixel spacing difference between the vehicle passing through each point for each point pair (e.g., A and B).

$$P_{AB} = | \text{Coords}_B - \text{Coords}_A | \tag{6}$$

where Coords_B and Coords_A are centers of points A and B, respectively. Finally, Equation (7) is used to calculate the distance in meters (d_{AB}).

$$d_{AB} = P_{AB} \times \text{PPM} \quad (7)$$

Four timestamps are stored when the vehicle passes the video frame columns to calculate the average speed. The average speed is calculated using the following equation (Equation (8)).

$$\text{Average Speed} = \frac{\frac{\Delta t_{AB}}{d_{AB}} + \frac{\Delta t_{BC}}{d_{BC}} + \frac{\Delta t_{CD}}{d_{CD}}}{3} \quad (8)$$

where Δt_{AB} is the timestamp between points a and b, Δt_{BC} is the timestamp between points b and c, and Δt_{CB} is the timestamp between points c and d in second. In this paper, based on mentioned equations, the improved VASCAR algorithm is implemented as a Python-based program in OpenCV, and the DNN is built. The program acts to detect the object as the vehicle detection and tracking, and then it tracks and estimates the speed as the vehicle speed estimation.

2.4. System Calibration

Some points should be considered while using a speed detector system camera. Pixel per meter ratio is one of the parameters which should be calibrated. It represents the slice of road covered by each pixel and is relative to the square distance from the camera. Notable factors include (a) camera height above ground (needs to be in the range of: distant (≥ 5 m) or close (< 5 m)), and (b) camera location (should be on the side of the road) [30]. Camera focal length is another important parameter mainly related to camera height, the length of the road segment, and the number of lanes covered by the field of view. In most related research, this number is reported as ≤ 25 mm [30] to cover multiple lanes and a large road stretch. Furthermore, system calibrations are carried out to better evaluate the proposed system and algorithms. This step is essential to tune system parameters and have some pre-analysis of the system. The calibration process contains the indoor and outdoor calibration from the tested FOV of the used camera to the program parameter and the final speed detection calibrated formula, which is described as follows:

2.4.1. Indoor System Calibration

Indoor system calibration extracts the camera's field of view (FOV). FOV is the maximum sample area that a camera can image. It is calculated in three steps (see Figure 6): horizontal, vertical, and diagonal. A diagonal field of view (DFOV) designates the diagonal dimensions of the measurement area in the object plane; a horizontal field of view (HFOV) defines the horizontal dimensions of the object plane, and a vertical field of view (VFOV) represents the vertical dimensions of the measurement area in the object plane [31].

As shown in Figure 6, to extract the maximum Pi camera FOV, the camera has been moved on along with points P and Q. Then, using Equation (9), the camera horizontal FOV value can be defined by:

$$\text{FOV} = 2 \tan^{-1} \left(\frac{1 \text{ image width}}{2 \text{ focal length}} \right) \quad (9)$$

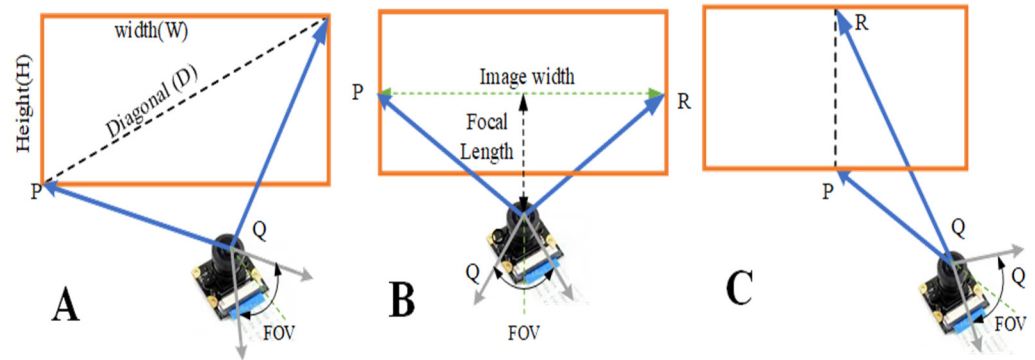


Figure 6. Different camera FOVs measurement situation, diagonal lengths (A), horizontal (B), and vertical (C).

FOV extraction includes the following steps based on the setup shown in Figure 6:

- Step 1: Calculates the horizontal, vertical, and diagonal FOV from a fixed distance from the object at different heights.
- Step 2: FOV extraction of the camera in different tilted positions on the x-axis to check any orientation effects on the Pi’s FOV.
- Step 3: FOV extraction of the camera in different tilted directions of the y-axis while the camera is 20 cm from the object. The same principle of the trapezoid as the last test applies, but in this case, the trapezoidal frame appears along the vertical side.
- Step 4: Finally, the camera performance was studied with a random test for any height and degree to calculate the FOV.

As Figure 6A shows, the camera system was put on top of the tilt systems to move the camera on various x- and y-axes. It should be mentioned that for each tilt, the trapezoidal area of the image gets changed (Figure 6B,C) [32]. Then, to calculate the FOV, the median of the trapezoidal (MT) image area is recalculated using the Equation (10).

$$MT = (L1 + L2)/2 \tag{10}$$

where L1 and L2 are the lengths of base 1 and 2, respectively, and MT (median of the trapezoid) is the image width used to calculate the FOV of the respective tilt angle.

Figure 7 shows the tilting system assembled with UAV and controlled with Raspberry Pi. As shown in Figure 7A, the assembled servo motor can move in ± 90 in X and Y directions. Figure 7B shows that changing the baseline of L1 and L2 can cause the three parallel situations. Figure 7C: horizontally angled. Figure 7D: vertically tilted, which can affect the acquired image by the camera. It should be mentioned that for the Outdoor test, the same assembly without a stand is installed on the top of the UAV.

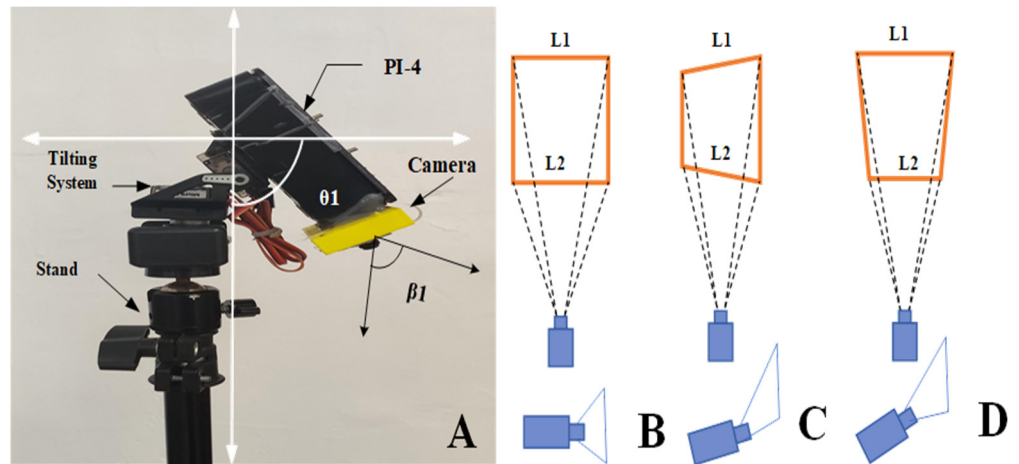


Figure 7. Indoor setup for the tilt system with the servo bed. (A) tilt system assembly, consisting of two servo motors capable of moving in the x and y axis along with raspberry PI 4B, pi camera. (B) the image and camera situation in a different scenario, parallel to the surface, (C) horizontally angled, (D) vertically tilted, L1: base 1 and L2: based 2.

2.4.2. Outdoor System Calibration

The whole setup was brought outside the lab and tested to find the best distance for object detection. The maximum distance was taken as the best distance because it would allow a single vehicle to traverse further in the frame. In each test, the FOV was recorded for the corresponding distance with the help of a measuring tape. The next step in outdoor system calibration is system parameter calibration. The max disappears, and distance and frame width should be correctly assigned to have the best system performance for different FOVs.

3. Experimentation and Results

3.1. Indoor System Calibration

The first indoor system calibration step was to find horizontal, vertical, and diagonal FOV from a fixed distance from the object at different heights. The experiment was conducted based on the setups shown in Figure 8.

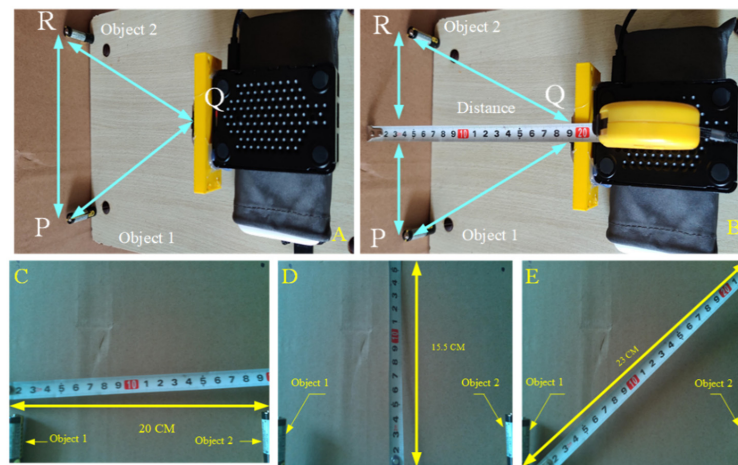


Figure 8. Indoor setup for horizontal, vertical, and diagonal FOV extraction from a fixed distance. (A): Distance between fixed object and camera, (B): Real Horizontal Length measurement, (C): Horizontal lengths inside the obtained image, (D): vertical lengths inside the obtained image, (E): diagonal lengths inside the obtained image.

To test the camera indoors FOV parameter, as the first step based on Figure 7, the Raspberry Pi with the camera mounted was set on a surface with a fixed object distance of 20 cm and varying height (r) from 0.25 to 3.5 m. The obtained results are shown in Table 1.

Table 1. Indoor FOV measurement with fixed distance (20 cm) and varying heights, Height (H), Horizontal Length (HL), Horizontal Fov (H_FOV), Vertical Length (VL), Vertical Fov (V_FOV), Diagonal Length (DL), Diagonal Fov (D_FOV).

H (m)	HL (cm)	H_FOV (Degree)	VL (cm)	V_FOV (Degree)	DL (cm)	D_FOV (Degree)
0.25	19.5	51.9784	15.5	42.3626	23	59.7978
0.5	19.6	52.2097	15.4	42.1134	23.2	60.2274
0.75	20	53.1301	14.9	40.8607	23.1	60.0128
1	20	53.1301	15	41.1120	22.8	59.3662
1.25	20.3	53.8155	15.2	41.6135	23.5	60.8684
1.5	19.8	52.6708	15.5	42.3626	23	59.7978
1.75	19.6	52.2097	15.3	41.8637	23	59.7978
2	20.3	53.8155	15.2	41.6135	23	59.7978
2.25	20.3	53.8155	15.2	41.6135	22.9	59.5822
2.5	20.1	53.3590	15.1	41.3630	23	59.7978
2.75	19.5	51.9784	15.1	41.3630	23	59.7978
3	20	53.1301	15.1	41.3630	23.1	60.0128
3.25	20.1	53.3590	15	41.1120	23	59.7978
3.5	19.9	52.9006	15	41.1120	23	59.7978

Table 1 concludes that the results of every test actually can coincide with the design FOV angles from the specifications (H_FOV: 53.50 +/- 0.13 degrees, V_FOV: 41.41 +/- 0.11 degrees) and considering that the 2-degree measurement error differential due to human error and the height does not affect the FOV by a huge margin, be it horizontal, vertical, or diagonal. It should be noted that because of the angle change, the image received or captured may seem rectangular on screen, detecting a trapezoidal frame. In the next step, the FOV variations in the fixed distance (20 cm) with different camera angles in the x-direction from -90 to +90 degrees are presented (Table 2).

Table 2. Indoor FOV (Filed Of View) measurement over changing the camera angle from -90 to +90 angle of view on the x-axis (AOV_X), Distance From Lens (DL), Horizontal Length (HL), Horizontal FOV (H_FOV), Vertical Length of Base 1 (VL1), VERTICAL LENGTH of BASE 2 (VL 2), Vertical Median of Trapezoidal Frame (VMT), Vertical FOV (V_FOV), Diagonal Length (DL), Diagonal FOV (D_FOV).

AOV_X (Degrees)	DL (cm)	H_L (Degree)	H_FOV (Degree)	VL1 (cm)	VL2 (cm)	VMT (cm)	V_FOV (Degree)	DI_L (cm)	D_FOV (Degree)
90									
75	Obj. out of scope	Null	0	Null	Null	Null	0	Null	0
60									
45	22.5	23	54.1441	15	18	16.5	40.272	35	75.7499
30	21.5	21	52.0591	15	17	16	40.819	32	73.3122
15	21	21	53.1301	15	15	15	39.307	30	71.0753
0	20	20	53.1301	15	15	15	41.112	23	59.7978
-15	21	21	53.1301	15	16	15.5	40.512	30	71.0753
-30	21.5	21	52.0591	15	17	16	40.819	32	73.3122
-45	22.5	21	50.0337	15	18	16.5	40.272	35	75.7499
-60									
-75	Obj. out of scope	Null	0	Null	Null	Null	0	Null	0
-90									

As Table 2 shows, for the degrees 60 or above, and in the same case for below -60, when the device was turned to that specific degree, the object's frame was out of the image frame. This test shows that the camera movement on the tillite system in the x direction

should be between ± 60 degrees. For the third test, the camera gradually tilted along the y-axis while the object was at 20 cm in a constant place. The same principle of the trapezoid as in the last test applies. In this case, the trapezoidal frame appears along the vertical side. It should be noted that due to the y-axis movement of the camera, only one base (base 2) of the image will be changed (Table 3).

Table 3 shows that the system has a limitation of ± 75 -degree rotation in the direction of the object inside the frame, so the direction of movement should rotate within ± 75 degrees. As the result shows, the degree between 75 and 90 in the Y direction with positive and negative values causes the camera disability to record an image, so the system loses its performance to track the object.

3.2. Outdoor System Calibration

The outdoor system calibration starts with checking the Pi camera FOV. In order to estimate vehicle speed accurately, the vehicle must be seen traversing from the initial point of the frame to the very end. Table 4 shows the various FOVs measured from various distances from 300 up to 1600 cm horizontally perpendicular to the road. All the outdoor system calibrations are conducted at a laminar wind speed.

Table 3. Indoor FOV measurement with device position from the object (cm) and changing the camera in the y direction, Distance From Lens (DL), Horizontal Length (HL), Horizontal FOV (H_FOV), the Vertical Length of base 1 (VL1), the vertical length of base 2 (VL2), Vertical Median of Trapezoidal Frame (VMT), Vertical FOV (V_FOV), Diagonal Length (DI_L), Diagonal FOV (D_FOV), object out shown as OUT.

AOV_Y (Degrees)	DL (cm)	VL2 (cm)	VMT (cm)	H_FOV (Degree)	VL1 (cm)	V_FOV (Degrees)	DI_L (cm)	D_FOV (Deg)
90	Obj. out of scope	Null	Null	0	Null	0	Null	0
75								
60	40	42	31	42.3626	16.1	29.113	39	64.342
45	34	36.5	28.25	45.1200	15.8	31.246	35	63.553
30	27	32	26	51.4199	15.5	33.196	32	63.215
15	24	27	23.5	52.1711	15.2	35.842	30	65.100
0	20	20	20	53.1301	15	41.112	23	59.797
-15	24	26.5	23.25	51.6887	15	35.757	30	65.657
-30	27	32	26	51.4199	15.4	32.993	32	63.215
-45	34	36	28	44.7602	15.6	31.132	35	64.010
-60	40	41.5	30.75	42.0510	15.9	28.991	39	64.761
-75	Obj. out of scope	Null	Null	0	Null	0	Null	0
-90								

Table 4. Outdoor Field Of View (FOV) measurement for various distances from the road, Average Horizontal Field Of View (AVG H_FOV).

Distance From Road (cm)	FOV (cm)	FOV (Degree)	AVG H_FOV (Degree)	FOV (Degree)
300	335	48.2	51.12	53.1
350	385	48.8		
400	430	48.8		
450	465	51.6		
500	515	51.7		
550	570	51.5		
600	570	53.5		
650	650	53.1		
700	770	51.53		
1600	1500	51.53		

In each test, the FOV was recorded for the corresponding distance with the help of a measuring tape. As Table 5 shows, the data obtained for the tested FOV are very close to the value declared by the camera manufacturer (53 degrees), which indicates the accuracy of the calculations and experiments. Finally, the last distance of 16 meters was set as the fixed distance for future tests due to the clear image visibility at this setup. At this distance, the FOV is 15 m.

Table 5. Final calibration of the system parameters.

Component	Description	Value (Unit)
max_disappear	Maximum consecutive frames for an object to be allowed to pass before deregistering it	15 frames
max_distance	Maximum distance between centroid to associate an object	1.75 m
track_object	Number of frames to track for object	4 frames
confidence	Minimum confidence or probability of detection	0.4
frame_width	Frame width in pixels	480 pixels
speed_estimation_zone	Speed estimation columns	4 (A, B, C, D)
distance	Distance from road to camera	16 m
speed_limit	Speed limit	To Be Set

3.3. System Software Parameters Calibration

As already mentioned, max disappears, max distance, track object, and frame width must be determined correctly for better system performance. The parameters have been calibrated through trial and outdoor experiments with the values, as presented in Table 5.

As shown in Table 5, the parameters used for max disappear and max distances are 15 and 1.75 m. The frame number for object tracking is set to 4. The confidence was chosen to be 0.4 (i.e., minimum detection percentage of 40%). This allows some flexibility because the model will also track objects it is less confident about. Since vehicles come in all shapes and sizes, this can increase robustness in real-world use. Frame width is set to 480 as both 60 fps and 90 fps footage are supported at this resolution. Moreover, it reduces computational needs and speeds up the process due to faster calculations on smaller images.

3.4. Vehicle Speed Estimation Optimization

A real vehicle test shows the difference between real speed and the system's estimated speed in two road directions and this difference is higher due to the greater distance of the quad from the road. To overcome this issue, as the last step, the final calibrated formula extracted (Equations (10) and (11)) with the help of curve fitting tools in MATLAB based on the following process is applied to the outcomes of the vehicle speed detection model. For this aim, the UAV was placed at a height of 3 m in the fixed point test, and a vehicle with a speed range of 10–70 km/h was used to test the system, considering the maximum speed limit of the city traffic police. A car with a driver and one of the researchers as an assistant driver was used. Before the vehicle starts to move, the driver is informed about the target speed then the driver brings the car's speed to the desired speed at the UAV location. Then, when passing the drone's position, along with checking vehicle identification, the UAV speed reading and the vehicle speed from the odometer are read and recorded by the driver's assistant. It should be noted that speed comparison is based on the two-way remark as direction 1, the path which has the minimum distance with the UAV and the vehicle is moving towards the UAV, and direction 2, going away from the UAV with the maximum distance and located on the other side of the street. The test is repeated five times, and the average is considered the final detected speed. Table 6 shows the system performance in real vehicle tests for the mentioned speed range.

Table 6. The real car speed and detected speed with the proposed system over different car directions (Direction 1: near side and Direction 2: faraway side).

Speed (km/h)	Direction 1 (y1)	Difference	Direction 2 (y2)	Difference
10	7.76	2.24	6.96	3.04
20	15.62	4.38	15.29	4.71
30	23.18	6.82	24.91	5.09
40	33.729	6.271	54.26	-14.26
50	43.1	6.9	32.83	17.17
60	73.08	-13.08	73.32	-13.32
70	83.22	-13.22	80.5	-10.5

The result shows that when the UAV is in the car’s direction side, the detected speeds are nearer than the cases with more than 16 m (Figure 9).

Figure 9 shows that the car has a different curve in each direction. Then, to have a better-speed estimation, the results from Table 7 were formulated with the help of the curve fitting tool in MATLAB software, and the extracted curve is shown in Equations (11) and (12).

$$y1 = (-2.283 \times 10^{-6})x^5 + (0.0004265)x^4 + (-0.0291)x^3 + (0.9024)x^2 + (-11.7)x + 59.67 \tag{11}$$

$$y2 = (-4.958 \times 10^{-6})x^5 + (0.001001)x^4 + (-0.07487)x^3 + (2.542)x^2 + (-37.01)x + 188.9 \tag{12}$$

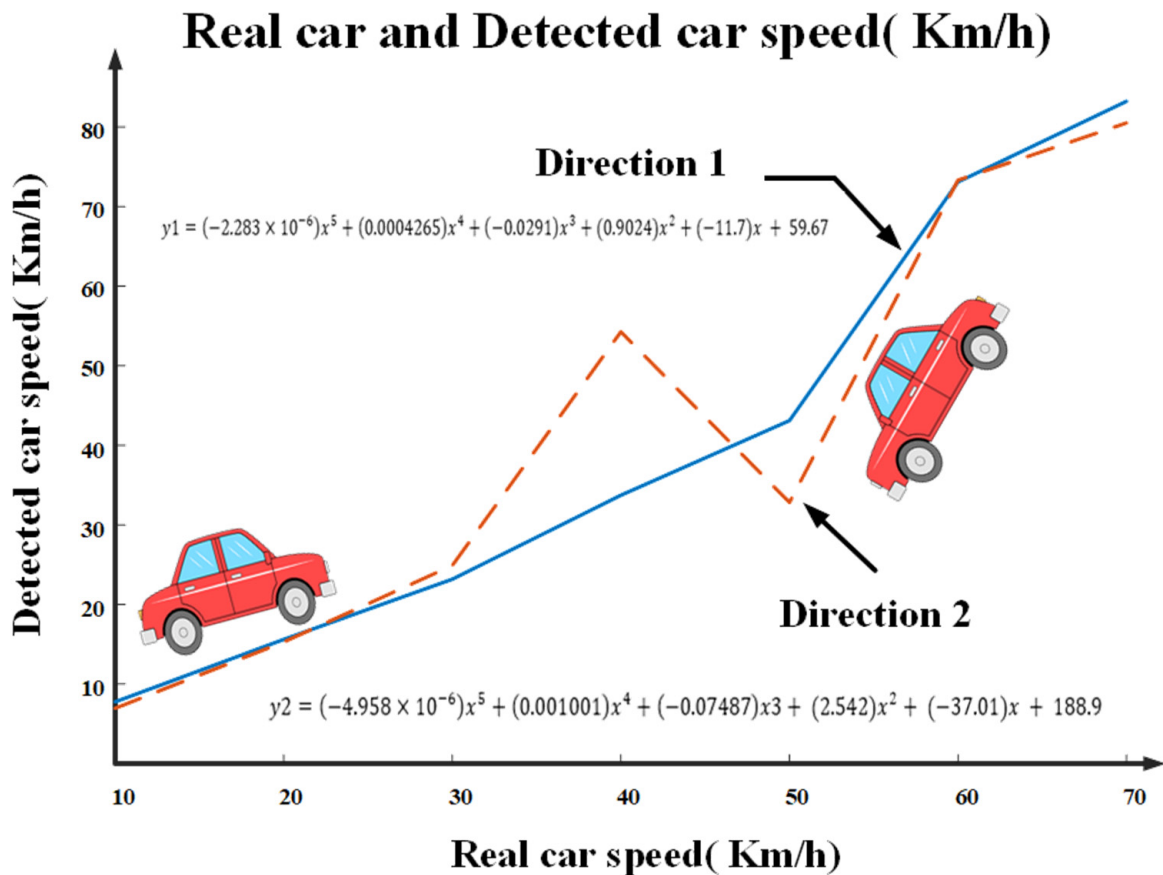


Figure 9. The measured and real vehicle speed differences in two directions.

Table 7. Vehicle Detection Accuracy on the UAV Height Variation.

UAV Height (m)	Number of Vehicles on Street	Number of Detected Vehicles	Detected Car (Error %)
0.7	32	42	31.25
1.0	19	24	26.32
1.25	25	31	24.00
1.50	32	38	18.75
1.75	34	40	17.65
2.50	34	38	11.76
3.0	34	38	11.76

As per as analysis in MATLAB with the mentioned coefficient in Equations (10) and (11), the best R2 for direction 1 is 0.9968 and for direction 2 is 0.9033.

3.5. Real Vehicle Test

The real vehicle test includes experiments regarding changes in UAV height from 0.7 to 3 m with the fixed location, changing the UAV degree with X-axis from -15 to $+15$, changing the camera degree with X-axis from -90 to $+90$, changing the camera degree with Y-axis from -90 to $+90$. Finally, a random test with dynamic height and degree was conducted (Figure 10). A vehicle was driven along a specific road (JXUST university golden campus, Ganzhou, China) with minimum traffic.

3.6. Vehicle Detection and Tracking

In the experiments, the car driver is asked to set a specific speed, so the real speed of the vehicle can be compared to the one obtained by the proposed system. In the first stage, the UAV was flown from 0.7 m height to 3 m. The maximum height of 3 m is assigned based on security issues. At each height, the estimated car speed was logged. The vehicle detection results on both roadsides are shown in Table 8.

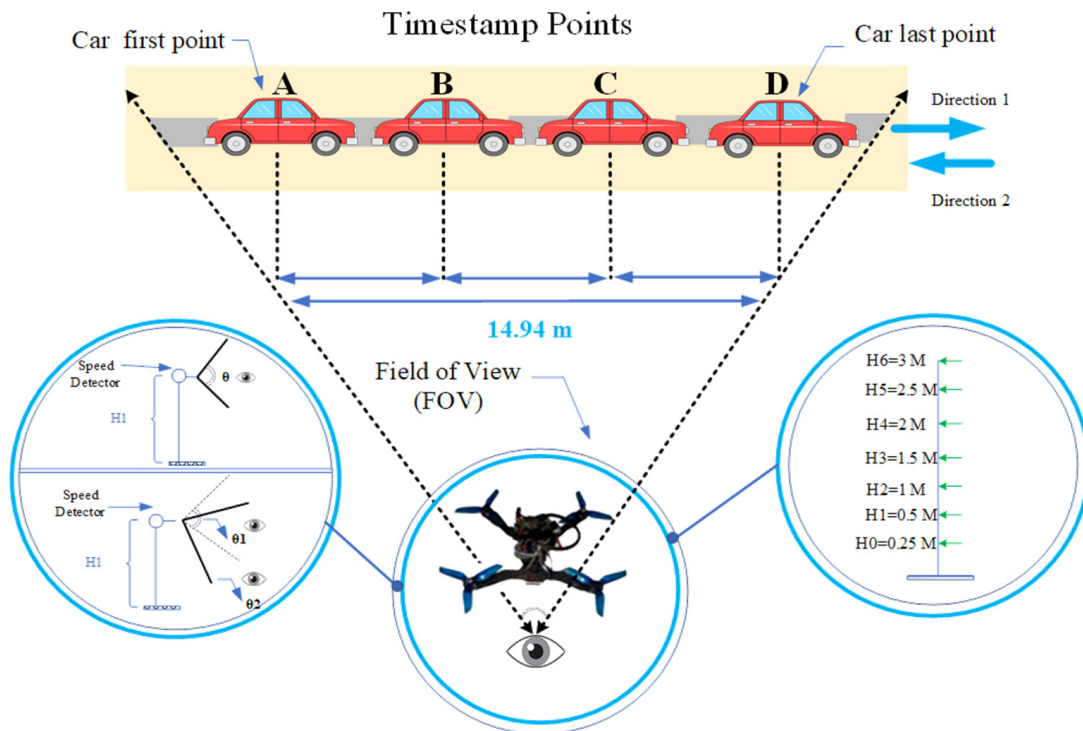


Figure 10. The schematic view of real vehicle tests with various location of A to D.

Table 8. Vehicle detection accuracy on the UAV X-axis degree variation.

X-Axis Change (Degree)	Number of Vehicles on Street	Number of Detected Vehicles	Detected Car (Error %)
−15	39	36	7.69
+15	26	30	15.38

In the next step, the car detection algorithm is tested when changing the UAV angle to the road with the x-axis from -15° to $+15^\circ$ at a UAV height of 3 m. The vehicle detection results on both roadsides are shown in Table 8.

The previous test is repeated for the changes in the Y-axis degree with the UAV height of 3 m. The results show that the UAV can monitor the road between +15 and -30 in the Y direction Table 9.

Table 9. Vehicle detection accuracy on the UAV y-axis degree variation.

Y-Axis Change (Degree)	Number of Vehicles on Street	Number of Detected Vehicles	Detected Car (Error %)
−30	22	28	27.27
−15	18	21	16.67
+15	21	25	19.05
+30	The road is out of range		

The last test is the system performance in a random situation with dynamic UAV height and a camera degree. This test in each step is repeated 5 times randomly, and the average is considered the final value is shown in Table 10.

Table 10. Vehicle detection accuracy on the system random test.

Random Parameter	Vehicles on Street (KM/h)	Detected Vehicles (KM/h)	Detection Error %
UAV height 1.5 m	49	58	18.37
UAV height 1.0 m	34	44	29.41
UAV height 2.0 m	42	46	9.52
x-axis -15 degree	36	39	8.33

4. Discussion

This research investigated low-amplitude UAV applications for car speed detection using Mobile Net-SSD models. Different indoor and outdoor tests were conducted to explore the camera's ability and calibrate the hardware. The special advantages of this design in low-altitude flights include battery energy consumption, reduced UAV charging speed, longer flight length, and the ability to develop a design to track vehicle speed at dynamic speed points, such as intersections, Joins of roads, traffic lights, etc. Another reason to check the vehicle's speed at a low height is to use a camera with fewer pixels and increase the UAV operating hours, as well as not interfere with the wind speed in the performance and control of the quad. In addition, this solution can be used in intersections and schools, kindergartens, and hospitals where vehicles generally accelerate at once. The system setup calibration demonstrated that a centroid tracking algorithm used for vehicle detection and tracking requires the camera to be perpendicular to the road to prevent obstacles. It seems that using any value for max disappear more than 15 with the given resolution of 640×480 would render speed detection impossible in most cases. Max distance higher than 175 cm could cause the centroid to disassociate from the object and fail to detect the vehicles.

Furthermore, it has been observed that heat substantially reduces the performance of the system. It affects the Intel neural compute stick (system shutdown due to the heat). The results show that vehicle detection error reduces when the UAV height increases. This means that by increasing the UAV height, vehicle overlapping decreases, and sudden

speed changes in vehicles can be detected easier. A system with a UAV positioned at lower heights leads to a loss in the system's tracking process. Experimental results of vehicle speed detection show that the minimum speed detection error obtained from a setup for the camera has a -15 -degree angle to the X-axis, and the maximum error is a -30 -degree angle. Another parameter which influences the system's accuracy is the distance from the road. As the vehicle moves further, the accuracy of vehicle detection reduces. This is especially critical for highways and wide roads because vehicles will not always drive along the road edge [33,34]. High-speed vehicles are more likely to avoid detection by the UAV speed detector. In addition, the speed of the vehicle is also one of the factors influencing the accuracy of the system, since vehicles do not always move at a constant speed. Sometimes, they may reduce speed to avoid a collision or react suddenly to a traffic situation. Moreover, vehicles are partly obscuring each other in a 2D frame due to their variable speeds. They sometimes stop in front of the camera and block other vehicles behind them. Final observations from the data show that any speed above 50 km/h reduces the system's performance. The UAV used in this project can also be autonomously controlled using modern trajectory planning algorithms, such as the evolutionary trajectory planning algorithm (ETPA), which is based on deep learning [35,36]. Besides the system can be equipped with pedestrian detection so that the UAV maintains its path avoiding pedestrians [37,38]. The mentioned improvement and utilization of modern technologies in making cities smart, especially in the transportation department, increases various parameters, such as the economy, environment, and infrastructure, from 10% to 30% [39]. Moreover, the data (image, video, graphics etc.) from these applications can help find behavior and support predictions using big data learning and discovery techniques [40].

5. Conclusions and Future Work

In this research paper, we have proposed a novel solution using extended UAVs, an application of remote sensing, to improve IoT-based smart city services. To show its superior performance, several different indoor and outdoor scenarios have been evaluated through implementation. The superior performance mainly stems from the accurate calibration of the UAV's camera, obtained in one of the implemented scenarios, supporting accurate vehicle speed detection. The results show that vehicle detection error reduces when the UAV height increases. Specifically, by increasing the UAV height, vehicles' separations are decreased, facilitating the easier detection of sudden speed changes in vehicles. Even in the case of connecting roads, such as the location of traffic lights, the car's speed generally varies, and sudden changes cause interference in the measurement of the actual speed, but the promising results of the solution elaborate on its effectiveness in crowded roads or junctions where vehicles have variant and non-stable speeds. In addition, our solution has the capability to connect to the traffic police with a friendly and easy-use GUI, which can handle the data and helps the end-users in the smart city to control the camera and record. In future work, we aim to evaluate it using the three different angles (yaw, pitch, roll) along with implementing other deep learning methods and comparing the measured system speed result with the city police control traffic cameras for better calibration and evaluation. It is also planned to check and average the vehicle's speed based on job distribution and a swarm of UAVs.

Author Contributions: Conceptualization: A.J.M., A.S.R., L.L., J.W. and A.T.; methodology: A.J.M., A.S.R., L.L. and J.W.; software: A.J.M., A.S.R. and L.L.; validation: A.J.M., A.S.R., L.L. and J.W.; investigation: A.J.M., A.S.R., L.L., J.W. and A.T.; resources: A.J.M., A.S.R. and L.L.; writing—original draft preparation: A.J.M., A.S.R., L.L., A.T. and J.W.; writing-review and editing: A.J.M., A.T., J.W. and M.G. All authors have read and agreed to the published version of the manuscript.

Funding: This work was supported by Jiangxi University of Science and Technology, 341000, Ganzhou, P.R China, underfunding numbers: 2021205200100563 (Corresponding author: Jianqing Wu).

Institutional Review Board Statement: Not applicable.

Informed Consent Statement: Not applicable.

Data Availability Statement: The data is available upon the request.

Conflicts of Interest: The authors declare no conflict of interest.

Nomenclature

AVG H_FOV	Average Horizontal Field Of View
Band	Band values
Coords _A	Centre of points A
Coords _B	Centre of points B
d(x, y)	Distance between x, y
d _{AB}	Distance in meters between A & B
d/t	Distance over time
DL	Distance From Lens
DI_L	Diagonal Length
D_FOV	Diagonal FOV
FOV	Field of View
HL	Horizontal Length
H_FOV	Horizontal FOV
Km/h	Kilometer per hour
L1	Length of base 1 of the trapezoidal image area
L2	Length of base 2 of the trapezoidal image area
MT	Median of the trapezoidal image area
NormBand	Normalized band
OUT	out object
PPM	Pixel per meter
P _{AB}	Pixel spacing between a & b
UAV	Unmanned aerial vehicle
VL1	the Vertical Length of base 1
VL2	the Vertical Length of base 2
VMT	Vertical Median of Trapezoidal Frame
V_FOV	Vertical FOV
μ _{BAND}	The mean of each red, green, and blue band
Δt _{AB}	Timestamp between a and b
σ	Scaling factor for normalization

References

1. Awais, M.; Li, W.; Cheema, M.J.; Hussain, S.; Shah, A.; Aslam, B.; Liu, C.; Ali, A. Assessment of optimal flying height and timing using high-resolution unmanned aerial vehicle images in precision agriculture. *Int. J. Environ. Sci. Technol.* **2021**, *19*, 2703–2720. [[CrossRef](#)]
2. Bennett, R.; van Oosterom, P.; Lemmen, C.; Koeva, M. Remote sensing for land administration. *Remote Sens.* **2020**, *12*, 2497. [[CrossRef](#)]
3. Moranduzzo, T.; Melgani, F. Car speed estimation method for UAV images. In *2014 IEEE Geoscience and Remote Sensing Symposium*; IEEE: Piscataway, NJ, USA, 2014; pp. 4942–4945. [[CrossRef](#)]
4. Cao, G.; Yang, X.; Li, H. Intelligent Monitoring System of Special Vehicle Based on the Internet of Things. In *Proceedings of International Conference on Computer Science and Information Technology. Advances in Intelligent Systems and Computing*; Patnaik, S., Li, X., Eds.; Springer: New Delhi, India, 2014; Volume 255. [[CrossRef](#)]
5. Carranza-García, M.; Torres-Mateo, J.; Lara-Benítez, P.; García-Gutiérrez, J. On the performance of one-stage and two-stage object detectors in autonomous vehicles using camera data. *Remote Sens.* **2020**, *13*, 89. [[CrossRef](#)]
6. Cepni, S.; Atik, M.E.; Duran, Z. Vehicle detection using different deep learning algorithms from image sequence. *Balt. J. Mod. Comput.* **2020**, *8*, 347–358. [[CrossRef](#)]
7. Deng, J.; Zhong, Z.; Huang, H.; Lan, Y.; Han, Y.; Zhang, Y. Lightweight Semantic Segmentation Network for Real-Time Weed Mapping Using Unmanned Aerial Vehicles. *Appl. Sci.* **2020**, *10*, 7132. [[CrossRef](#)]
8. Coombes, M.; Fletcher, T.; Chen, W.H.; Liu, C. Decomposition-based mission planning for fixed-wing UAVs surveying in wind. *J. Field Robot.* **2020**, *37*, 440–465. [[CrossRef](#)]
9. Du, M.; Noguchi, N. Monitoring of Wheat Growth Status and Mapping of Wheat Yield's within-Field Spatial Variations Using Color Images Acquired from UAV-camera System. *Remote Sens.* **2017**, *9*, 289. [[CrossRef](#)]
10. García, L.; Parra, L.; Jimenez, J.M.; Lloret, J.; Mauri, P.V.; Lorenz, P. DronAway: A Proposal on the Use of Remote Sensing Drones as Mobile Gateway for WSN in Precision Agriculture. *Appl. Sci.* **2020**, *10*, 6668. [[CrossRef](#)]

11. Ibrar, M.; Mi, J.; Karim, S.; Laghari, A.A.; Shaikh, S.M.; Kumar, V. Improvement of Large-Vehicle Detection and Monitoring on CPEC Route. *3D Res.* **2018**, *9*, 45. [CrossRef]
12. Døssing, A.; Lima Simoes da Silva, E.; Martelet, G.; Maack Rasmussen, T.; Gloaguen, E.; Thejll Petersen, J.; Linde, J. A High-Speed, Light-Weight Scalar Magnetometer Bird for km Scale UAV Magnetic Surveying: On Sensor Choice, Bird Design, and Quality of Output Data. *Remote Sens.* **2021**, *13*, 649. [CrossRef]
13. Huang, Y.; Thomson, S.J.; Brand, H.J.; Reddy, K.N. Development and evaluation of low-altitude remote sensing systems for crop production management. *Int. J. Agric. Biol. Eng.* **2016**, *9*, 1–11. [CrossRef]
14. Jaiswal, D.; Kumar, P. Real-time implementation of moving object detection in UAV videos using GPUs. *J. Real-Time Image Proc.* **2020**, *17*, 1301–1317. [CrossRef]
15. Lenain, L.; Melville, W.K. Autonomous surface vehicle measurements of the ocean's response to Tropical Cyclone Freda. *J. Atmos. Ocean. Technol.* **2014**, *31*, 2169–2190. [CrossRef]
16. Park, S.S.; Kozawa, K.; Fruin, S.; Mara, S.; Hsu, Y.-K.; Jakober, C.; Winer, A.; Herner, J. Emission factors for high-emitting vehicles based on on-road measurements of individual vehicle exhaust with a mobile measurement platform. *J. Air Waste Manag. Assoc.* **2011**, *61*, 1046–1056. [CrossRef] [PubMed]
17. Afifah, F.; Nasrin, S.; Mukit, A. Vehicle Speed Estimation using Image Processing. *J. Adv. Res. Appl. Mech.* **2019**, *48*, 9–16. Available online: http://www.akademiabaru.com/doc/ARAMV48_N1_P9_16.pdf (accessed on 10 July 2022).
18. Sadeghi, M.; Emadi Andani, M.; Bahrami, F.; Parnianpour, M. Trajectory of Human Movement during Sit to Stand: A New Modeling Approach Based on Movement Decomposition and Multi-Phase Cost Function. *Exp. Brain Res.* **2013**, *229*, 221–234. [CrossRef] [PubMed]
19. Zhang, X.; Yang, G.; Liu, S.; Moshayedi, A.J. Fractional-order circuit design with hybrid controlled memristors and FPGA implementation. *AEU-Int. J. Electron. Commun.* **2022**, *153*, 154268. [CrossRef]
20. Intel. Intel® Movidius™ Myriad™ X Vision Processing Unit. Available online: <https://www.intel.com/content/www/us/en/products/details/processors/movidius-vpu/movidius-myriad-x.html> (accessed on 10 July 2022).
21. Moshayedi, A.J.; Roy, A.; Liao, L.; Li, S. Raspberry Pi SCADA Zonal based System for Agricultural Plant Monitoring. In Proceedings of the 2019 6th International Conference on Information Science and Control Engineering (ICISCE), Shanghai, China, 20–22 December 2019; pp. 427–433. [CrossRef]
22. Gay, W. Pi Camera. In *Advanced Raspberry Pi*; Apress: Berkeley, CA, USA, 2018. [CrossRef]
23. Jian, Z.; Yonghui, Z.; Yan, Y.; Ruonan, L.; Xueyao, W. MobileNet-SSD with the adaptive expansion of the receptive field. In Proceedings of the 2020 IEEE 3rd International Conference of Safe Production and Informatization (IICSPI), Chongqing, China, 28–30 November 2020; pp. 177–181. [CrossRef]
24. Ren, J.; Li, H. Implementation of Vehicle and License Plate Detection on Embedded Platform. In Proceedings of the 2020 12th International Conference on Measuring Technology and Mechatronics Automation (ICMTMA), Phuket, Thailand, 28–29 February 2020; pp. 75–79. [CrossRef]
25. Chiu, Y.C.; Tsai, C.Y.; Ruan, M.D.; Shen, G.Y.; Lee, T.T. Mobilenet-SSDv2: An Improved Object Detection Model for Embedded Systems. In Proceedings of the 2020 International Conference on System Science and Engineering (ICSSE), Kagawa, Japan, 31 August–3 September 2020; pp. 1–5. [CrossRef]
26. Xu, G.; Khan, A.S.; Moshayedi, A.; Zhang, X.; Shuxin, Y. The Object Detection, Perspective and Obstacles In Robotic: A Review. *EAI Endorsed Trans. AI Robot.* **2022**, *1*, e13. [CrossRef]
27. Gao, C.; Zhai, Y.; Guo, X. Visual Object Detection and Tracking System Design based on MobileNet-SSD. In Proceedings of the 2021 7th International Conference on Computer and Communications (ICCC), Chengdu, China, 10–13 December 2021; pp. 589–593. [CrossRef]
28. Zhang, J.; Xu, J.; Zhu, L.; Zhang, K.; Liu, T.; Wang, D.; Wang, X. An improved MobileNet-SSD algorithm for automatic defect detection on vehicle body paint. *Multimed. Tools Appl.* **2020**, *79*, 23367–23385. [CrossRef]
29. Prakash, N.; Kamath, C.; Gururaja, H.S. Detection of traffic violations using moving object and speed detection. *Wutan Huatan Jisuan Jishu* **2020**, *16*, 1001–1749.
30. Fernández Llorca, D.; Hernández Martínez, A.; García Daza, I. Vision-based vehicle speed estimation: A survey. *IET Intell. Transp. Syst.* **2021**, *15*, 987–1005. [CrossRef]
31. Haldar, S.K. Field of View. Available online: <https://www.sciencedirect.com/topics/earth-and-planetary-sciences/field-of-view> (accessed on 10 July 2022).
32. Schwager, M.; Julian, B.; Angermann, M.; Rus, D. Eyes in the Sky: Decentralized Control for the Deployment of Robotic Camera Networks. *Proc. IEEE* **2011**, *99*, 1541–1561. [CrossRef]
33. Mishra, D.; Khan, A.; Tiwari, R.; Upadhyay, S. Automated Irrigation System-IoT Based Approach. In Proceedings of the 2018 3rd International Conference On Internet of Things: Smart Innovation and Usages (IoT-SIU), Bhimtal, India, 23–24 February 2018; pp. 1–4. [CrossRef]
34. Tiwari, R.; Sharma, H.K.; Upadhyay, S.; Sachan, S.; Sharma, A. Automated parking system-cloud and IoT based technique. *Int. J. Eng. Adv. Technol. (IJEAT)* **2019**, *8*, 116–123.
35. Asim, M.; Mashwani, W.K.; Shah, H.; Belhaouari, S.B. An evolutionary trajectory planning algorithm for multi-UAV-assisted MEC system. *Soft Comput.* **2022**, *26*, 7479–7492. [CrossRef]

36. Asim, M.; Mashwani, W.; Belhaouari, S.; Hassan, S. A Novel Genetic Trajectory Planning Algorithm With Variable Population Size for Multi-UAV-Assisted Mobile Edge Computing System. *IEEE Access* **2021**, *9*, 125569–125579. [[CrossRef](#)]
37. Iftikhar, S.; Zhang, Z.; Asim, M.; Muthanna, A.; Koucheryavy, A.; Abd El-Latif, A.A. Deep Learning-Based Pedestrian Detection in Autonomous Vehicles: Substantial Issues and Challenges. *Electronics* **2022**, *11*, 3551. [[CrossRef](#)]
38. Iftikhar, S.; Asim, M.; Zhang, Z.; El-Latif, A.A.A. Advance generalization technique through 3D CNN to overcome the false positives pedestrian in autonomous vehicles. *Telecommun. Syst.* **2022**, *80*, 545–557. [[CrossRef](#)]
39. Nguyen, D.D.; Rohács, J.; Rohács, D.; Boros, A. Intelligent total transportation management system for future smart cities. *Appl. Sci.* **2020**, *10*, 8933. [[CrossRef](#)]
40. Gao, Z.K.; Liu, A.A.; Wang, Y.; Small, M.; Chang, X.; Kurths, J. IEEE Access Special Section Editorial: Big Data Learning and Discovery. *IEEE Access* **2021**, *9*, 158064–158073. [[CrossRef](#)]

Disclaimer/Publisher’s Note: The statements, opinions and data contained in all publications are solely those of the individual author(s) and contributor(s) and not of MDPI and/or the editor(s). MDPI and/or the editor(s) disclaim responsibility for any injury to people or property resulting from any ideas, methods, instructions or products referred to in the content.